15th Australasian Fluid Mechanics Conference
The University of Sydney, Sydney, Australia
13-17 December 2004

Computing Turbulent Channels at Experimental Reynolds Numbers

J. Jiménez[1,2] **and J.C. del Álamo**[1]

[1]School of Aeronautics, Universidad Politécnica
28040 Madrid, SPAIN

[2]Centre Turbulence Research, Stanford University
Stanford CA, 94305, USA

Abstract

The availability of high-quality numerical simulations, with Reynolds numbers which are now in the range of $Re_\tau = 2000$, and which will probably be extended to $Re_\tau \approx 4000$ in the near future, have revitalized the study of turbulence near walls in the last decade. Simulations can now be used to study the dynamics of the buffer and of the lower logarithmic layers in some detail, and some of the results obtained in that way are reviewed here. Particular attention is paid to the reasons for the failure of the scaling of the turbulence intensities with u_τ, which are traced to different causes in the buffer layer and in the outer flow. While in the buffer layer the cause seems to be the growing scale disparity between the near-wall and outer-flow contributions, it is shown that in the outer flow some spectral ranges scale with the centreline velocity. The generation of the largest scales of the streamwise velocity component in the logarithmic layer is also studied, and shown to be consistent with the formation of large-scale passive wakes of smaller individual ejections. The latter are related to attached clusters of vortices extending from the buffer region into the logarithmic layer.

Introduction

The study of turbulence near walls has experienced a renaissance in the last decade, largely because of the availability of high-quality numerical simulations. The numerical Reynolds numbers, now in the range of $Re_\tau = 2000$, allow for the first time the study in some detail of the dynamics of the buffer and of the lower logarithmic layers. The present and probable future status of direct simulations of turbulent channels, and some of the results obtained from them, are reviewed here.

Three issues are particularly addressed. Consider first the buffer and viscous layers. It has been known for some time that this part of the flow is relatively independent of the flow above it [17], and actually survives even when all the rotational fluctuations are artificially removed above $y^+ \approx 60$. This is in agreement with the fact that most of the mean velocity difference, of the turbulence production, and of the energy dissipation, reside in this region, which therefore sees the outer flow as a relatively weak perturbation of the local processes. These autonomous dynamics have been discussed elsewhere [9, 11, 15, 16], and will not be addressed here, but recent experimental results suggest that there are effects of the Reynolds number on the scaling of buffer-layer quantities [7]. They can only come from interactions with the outer flow, and they are also seen in simulations. We will review below some results obtained in the last few years, concerning their mechanism and their location in scale space.

The next question is the scaling of the structures both in the buffer and in the logarithmic layer. It follows from the study of the numerical energy spectra that the relation between the width and the length of the energy-containing structures is not straightforward, in the sense that both length scales are not proportional to each other, nor to the distance to the wall. Experimental evidence for the latter lack of proportionality had already been found in [12, 19], but it has only been through numerical simulations that the former has been documented [2, 3, 14]. We will discuss below what the problem is, and what its solution appears to be.

Finally we address the question of the scaling of the velocity fluctuations in the logarithmic layer and in the outer layer. The classical view is that all the velocity fluctuations in wall flows should scale with the friction velocity u_τ [30], but again the experimental evidence suggests otherwise [7], and it had already been noted in [31] that 'inactive' eddies, those not carrying Reynolds stresses, could scale in some other way. We will show that at least some eddies, those large enough to span the whole thickness of the flow, scale with the flow velocity at the centreline, and we will discuss the consequences that follow for the behaviour of the overall turbulence intensities at very high Reynolds numbers.

We use x, y and z for the streamwise, wall-normal, and spanwise coordinates, and u, v and w for the corresponding velocity components. The half-height of the channel, the pipe radius, and the boundary-layer thickness are denoted by h.

Numerical simulations

There should be by now little doubt that careful numerical simulations of the Navier–Stokes equations are just different kinds of experiments, and that there is no reason to expect them to be less accurate than laboratory ones [23]. Some of their drawbacks, such as the artificial nature of some boundary conditions, are no worse than the artificial nature of the walls in wind tunnels and can, in both cases, be avoided by careful design. It is also not always clear that what we simulate is exactly the same thing that we would measure in the laboratory, but there is no reason why it should be. Simulations and experiments are equally valid idealizations against which to test theories and designs.

There is also no doubt that, once a flow has been successfully simulated, it can be observed more thoroughly than in a laboratory experiment. The cost of carrying out a large simulation is high, although not necessarily higher than that of building a large wind tunnel, but the instrumentation problems are simpler, and almost any observation that can be imagined can be made. While the results of laboratory experiments are often constrained by the instrumentation technology, those from numerical simulations are mainly limited by the ability of the researcher to ask the right questions.

Another advantage of simulations over laboratory experiments is the ease with which they can be adapted to perform 'conceptual' experiments, in which the equations of motion or the boundary conditions are changed to, in effect, 'take the system apart' [17]. This has always been a useful device in physics, and conceptual experiments have often been used to constrain physical theories by asking what would happen if a given 'im-

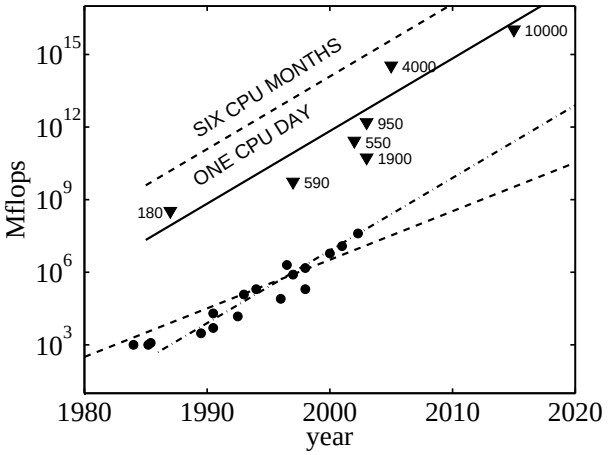

Figure 1: Evolution of direct channel simulations. ● , peak speeds of computers, in Mflops/s, as a function of the fabrication year. The two trend lines are for single- and multi-processor systems. The two upper lines are for total flops in one day and in six months of dedicated time at the computational speeds of the parallel trend line. ▼ are the estimated costs of the simulations in table 1.

Re_τ	**Box**	**Year**	**Points**
180	$4\pi \times 4\pi/3$	1987 [21]	5 Mp
590	$2\pi \times \pi$	1996 [24]	40 Mp
550	$8\pi \times 4\pi$	2001 [2]	600 Mp
950	$8\pi \times 3\pi$	2003 [3]	4 Gp
1900	$\pi \times \pi/2$	2003 [3]	450 Mp
4,000	$8\pi \times 3\pi$	2005	130 Gp
10,000	$8\pi \times 3\pi$	2015	1.5 Tp

Table 1: Available and planned direct numerical simulations of turbulent channels. The box refers to the spatial periodicity of the spectral simulation contained in the table.

plausible' modification were implemented. Think for example of the concept of potential inviscid flow. For such exercises to be useful, however, we should be able to answer the question that we have posed, and it is in that respect that many of the idealized systems of classical physics differ from complex ones, such as turbulence. While it might be possible with a pencil and paper, and with a lot of imagination, to decide what happens when two observers try to synchronize their clocks under certain conditions, the answer is often harder when trying to decide the outcome of a particular modification to a turbulent flow. Numerical simulations allow us to obtain answers to our conceptual experiments.

While those are clear advantages of simulations over laboratory experiments, the argument over their relative merits has often centred on the different question of which systems can be studied with each technique. It is often claimed that experiments can be run at higher Reynolds numbers than simulations. This question was reviewed in [13], where it was argued that the Reynolds number difference between laboratory and computation has been steadily eroding with the advances in computing technology, and that in many respects both are now comparable. This is particularly true when the magnitude of interest is something more complicated than the turbulence intensities, or even in some cases anything beyond the mean velocity profile.

In the particular case of turbulent channels, which will be the main subject of this paper, the friction Reynolds numbers of the early simulations at $Re_\tau = u_\tau h/\nu = 180$ [21] have now been multiplied by five [3]. A simulation at $Re_\tau \approx 2000$ is also available, although the size of its computational box is too small to trust the results anywhere except very near the wall. The available simulations are summarized in table 1, and they overlap the experimental range. There are few well-documented laboratory channels at $Re_\tau > 1000$, and the main problem in validating the results of the simulations is now the lack of comparable experimental data.

The cost of these simulations is plotted in figure 1 against the historical and expected evolution of computer power. They cluster around one CPU-day of the fastest machine available at the time, showing that the barrier for larger simulations is more political than technological. None of the simulations in the figure were ran in the fastest available machine.

Two simulations still in the planning stage are included in table 1. The one at $Re_\tau = 4000$ is at present in the advanced preparation phase, and will most probably be ready within the next two years. The simulation at $Re_\tau = 10^4$ is a more distant prospect, but it holds a special place in the planing process. The two main 'intrinsic' open problems in wall-bounded turbulence are the interaction between the inner and the outer layers, and the dynamics of the logarithmic layer. Both require a sufficiently large Reynolds number.

The length of the dominant structures in the buffer layer is about 1000 wall units [14], while that of the global modes in the outer region is about five channel half-widths [2]. When $Re_\tau = 10^4$, the ratio between the two lengths is about 50, and probably large enough to be considered infinite from the point of view of their interaction. That Reynolds number also results in about a factor of ten between the upper and lower limits of the logarithmic layer [25]. Such a simulation can probably be considered as 'asymptotically large' from the point of view of clarifying the physics of wall-bounded flows at zero pressure gradient. It should be ready in about a decade.

It may be interesting at this point to discuss the question of the size of the computational box needed to simulate channels. We will see below that there are very long structures in turbulent wall-bounded flows, particularly for the streamwise velocity component, which contain a substantial fraction of the energy of the fluctuations. As long as the physics of those large scales, and of their interactions with other parts of the flow, is not completely understood, they have to be simulated to have any confidence in the results. As we will see below, this understanding has been achieved only in part, and many of the resulting scaling laws are still in doubt. Any new simulation at large Reynolds numbers, which is bound to be expensive and not easily repeated for some time, should use boxes large enough to include them.

With this in mind, there are still many things that can be learned from smaller boxes, in particular regarding the dynamics of the smaller scales in the absence of the larger ones [16, 17]. Something that usually does not work, however, is to use smaller computational boxes to save computer time. Consider for example the simulations in table 1. It is our experience that boxes in the order of $L_x = 8\pi$ need to be run for about ten washouts $(10L_x/U_c)$ before the statistics of the larger scales are reasonably converged. Smaller boxes need to be run much longer, in part to accumulate enough statistics at the intermediate scales, and also because there is a tendency for the long Fourier modes in the centre of the channel to become 'frozen', producing spurious effects on the velocity fluctuation profiles which are not necessarily small. The problem is that short periodic boxes do not really lack long scales, but merely treat them as being in-

finitely long. The scales are in the simulation, but their dynamics are in general incorrect.

The box at $Re_\tau = 1880$ in table 1, for example, had to be run for several hundred washouts before its statistics could be considered moderately converged. Even then the mean velocity profile cannot be trusted above the logarithmic layer. The same is true of the somewhat larger box at $Re_\tau = 590$, which also had to be run for hundreds of washouts before converging, and which even so retained a residual asymmetry in the velocity profile at the end of the simulation [24, private communication]. Our experience with intermediate boxes of size $4\pi \times 2\pi$ is that they have to be run for about $80-100$ washouts before the statistics converge in the outer region. These long integration times negate much of the gain in computer time which could be expected from using smaller boxes (although obviously not in memory usage), and they do so at the expense of decreasing the quality of the results. The consequence is that it usually pays to run the largest computational box compatible with the computer resources at hand, and that the main reason to use smaller boxes should be to simplify the physics, rather than to shorten the simulation time.

The near-wall layer

It is well known [30] that wall-bounded turbulence over smooth walls can be described to a good approximation in terms of two sets of scaling parameters. Viscosity is important near the wall, and the length and velocity scales in that region are constructed with the kinematic viscosity ν and with the friction velocity u_τ. Everything in that region is expected to scale in wall units.

Far from the wall the velocity also scales with u_τ, but the length scale is the flow thickness h. In the classical approximation the logarithmic region extends between the inner and the outer regions, because the only possible length scale is then y itself [30]. The velocity in the intermediate layer follows approximately

$$U^+ = \kappa^{-1} \log y^+ + A. \qquad (1)$$

The viscous and buffer layers are extremely important for the flow as a whole. The ratio between the inner and outer length scales is the friction Reynolds number, Re_τ, which ranges from 200 for barely turbulent flows to $Re_\tau = 5 \times 10^5$ for large water pipes. The near-wall layer in the latter, $y^+ \lesssim 150$, is only about 3×10^{-4} times the pipe radius, but it follows from (1) that, even in that case, 40% of the velocity drop takes place below $y^+ = 50$. Turbulence is characterized by the expulsion towards the small scales of the energy dissipation, away from the large energy-containing eddies. In wall-bounded flows that separation occurs not only in scale space for the velocity fluctuations, but also in the mean velocity profile. The singularities are expelled both from the large scales, and from the centre of the flow towards the wall.

Because of this singular nature, the near-wall layer is not only important for the rest of the flow, but it is also essentially independent from it. That was for example shown by numerical experiments with 'autonomous' simulations [17] in which the outer flow was artificially removed above a certain wall distance δ. The near-wall dynamics were unaffected as long as $\delta^+ \gtrsim 60$.

Understanding the structure of this part of the flow has practical implications. The velocity at the centreline, $U_c^+ = (2/c_f)^{1/2}$, determines the friction coefficient c_f when expressed in wall units, and we have seen than a large fraction of that velocity resides in the buffer layer. It is for this reason that the layer below $y^+ \approx 100$ has been intensively studied. It is dominated by coherent streaks of the streamwise velocity and by quasi-streamwise vortices. The former are an irregular array of long

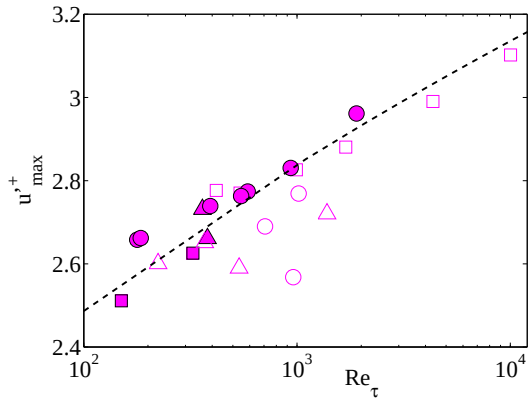

Figure 2: Maximum intensity of the streamwise velocity fluctuations as a function of the Reynolds number. In all cases the maximum is achieved near $y^+ = 15$. □ , boundary layers; ○ , channels; △ , pipes. Open symbols are laboratory experiments, and closed ones are computations. The dashed line is $u'^{+2} \sim \log(20 Re_\tau)$.

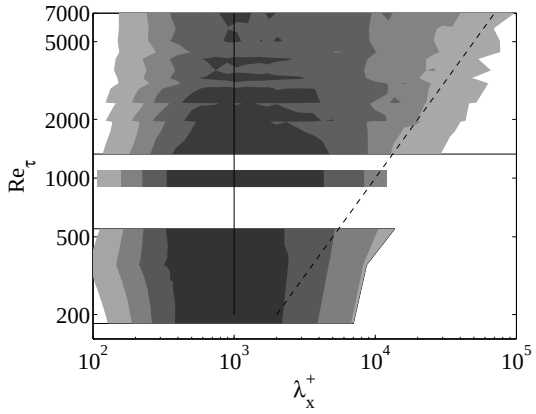

Figure 3: Longitudinal energy spectra $k_x E_{uu}/u_\tau^2$ as a function of the wavelength $\lambda_x = 2\pi/k_x$, and of the Reynolds number, at $y^+ = 20$. Each horizontal line of the shaded area corresponds to a different Reynolds number. The upper block are laboratory boundary layers [10]. The lower one are numerical channels [2, 3]. The dashed line is $\lambda_x = 10h$, and the solid one is $\lambda_x^+ = 1000$. Adapted from [14].

$(x^+ \approx 1000)$ sinuous alternating streamwise jets superimposed on the mean shear, with an average spanwise separation of the order of $z^+ \approx 100$ [29]. The quasi-streamwise vortices are slightly tilted away from the wall [11], and stay in the near-wall region only for $x^+ \approx 200$. Several vortices are associated with each streak, with a longitudinal spacing of the order of $x^+ \approx 400$. The basic cell of wall-parallel dimensions 400×100 wall units was also identified in [16] as the smallest dynamical periodic box able to self-sustain turbulence in the neighbourhood of the wall.

The intensity of the streamwise velocity fluctuations reaches a maximum around $y^+ \approx 15$, and classical theory implies that the maximum intensity should scale in wall units. It is clear from figure 2 that this is not true, and that the increasing trend is present both in the experimental and in the numerical results. This anomalous scaling is accompanied by other scaling failures in the buffer region. The most obvious is the form of the premultiplied energy spectrum, which was shown in [10] to contain two peaks, a short one at a streamwise wavelength $\lambda_x^+ \approx 1000$,

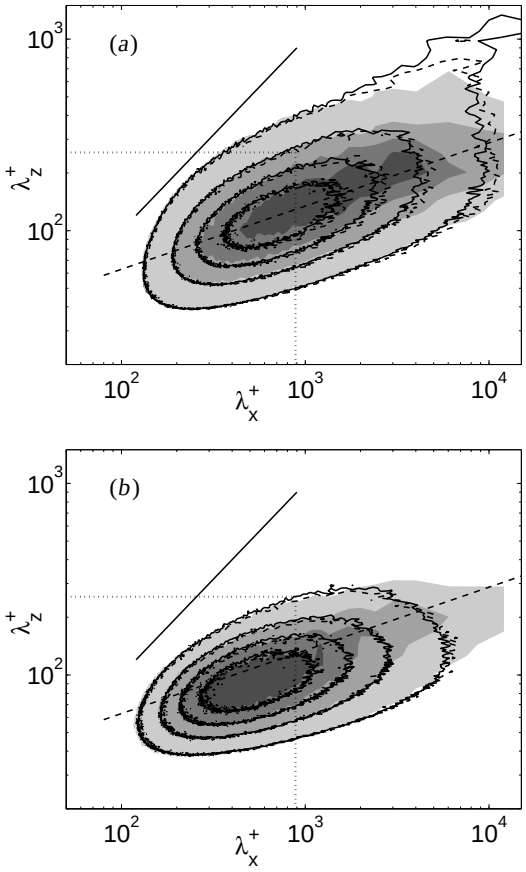

Figure 4: Two-dimensional spectral energy densities at $y^+ = 16$, in terms of the streamwise and spanwise wavelengths. Shaded contours are an autonomous flow [14] masked above $y^+ = 60$. Lines are full channels [3]. – – – – , $Re_\tau = 550$; ——— , $Re_\tau = 934$. The solid diagonal line is horizontal isotropy, $\lambda_x = \lambda_z$, and the dashed one is $\lambda_z \sim \lambda_x^{1/3}$. The dotted rectangle is the approximate size of the minimal self-sustaining flow unit [16]. (*a*) $k_x k_z E_{uu}/u_\tau^2$. (*b*) $-k_x k_z E_{uv}/u_\tau^2$.

independent of Re_τ, and a long one that scales in outer units as $\lambda_x \approx 10h$. A compilation of experimental and numerical spectra is found in figure 3. Since u'^2 is the integral of the energy spectrum, a nonclassical scaling of the latter almost automatically implies a similar nonclassical behaviour of the former.

The Reynolds-number dependence of the large scales can be also be seen in figure 4, which shows two-dimensional energy densities in the near-wall region. These spectra have at least three regions. On the lower left corner, at scales of the order of the minimum flow unit mentioned above, the two Reynolds numbers in the figure collapse well in wall units, and so does the autonomous flow that is also included. These are the structures involved in the nonlinear turbulence regeneration cycle, and they are present both in the spectrum of the energy and in that of the Reynolds stress. Both spectra continue towards longer wavelengths along a ridge with the anomalous power scaling $\lambda_z \sim \lambda_z^{1/3}$, which is present in the three flows. At the Reynolds numbers of the present simulations this spectral range also collapses in wall units, but the autonomous flow behaves differently, and it is not clear from the present data whether the ridge will become longer at higher Reynolds numbers, or whether the present data are already asymptotic. It was shown in [14] that the structures in this ridge are passive, in the sense that they are not involved in a two-way cycle. Their wall-normal velocity is needed to create the streamwise-velocity structures, but not the other way around. It was also shown in [14] that the geometric relation between the smaller *v* structures in the minimal region and the longer *u*-structures along the ridge is consistent with the latter being wakes of the former. Their scaling is also consistent with this explanation. The similarity solution for wakes spreading in a simple shear under the action of a constant viscosity, both of which are good approximations near the wall, is

$$u \sim u(y/x^{1/3}, z/x^{1/3}). \tag{2}$$

Further support for the wake model will be provided in the next section.

The spectral region in which the three flows disagree most clearly is the upper right-hand corner, where the spectrum of the higher Reynolds number flow is longer and wider than that of the lower one. This component is completely absent in the autonomous flow, and is located around $\lambda_x \times \lambda_z = 10h \times h$. Its length thus agrees with the long-wavelength end of the spectra in figure 3. It is also the location of the 'global' modes identified in [2], which span the whole channel half-height and which will be the subject of a later section.

This strongly suggests that the growth of the intensity peak in figure 2 is due to large-scale outer flow structures. Note that, contrary to the other two spectral regions, this component is not present in the Reynolds-stress cospectrum, and is therefore 'inactive' in the sense of Townsend [31]. It has long been understood that, because the Reynolds stress defines u_τ, the most likely reason for the failure of the wall scaling is the presence of inactive motions [31], and this is confirmed by the excellent collapse of the two full-channel cospectra in figure 4(*b*).

Note however that this correspondence is not automatic. The edge of the energy spectrum in figure 4(*a*) which is closest to the isotropic diagonal is missing in the cospectrum, but it scales very well in wall units.

Wakes in the logarithmic region

As we move away from the wall, the form of the energy spectrum changes [2, 3]. Two spectra are shown in figure 5. The ridge of 'wakes' is also present in them, but it follows

$$\lambda_z \approx (y\lambda_x)^{1/2}, \tag{3}$$

rather than a cube-root law found in the viscous layer. This is also consistent with the model of a wake left by a compact structure, because in the logarithmic and outer layer the velocity is almost constant, and the diffusion of the wake is due to an eddy viscosity which, on dimensional grounds, is $\nu_T \approx u_\tau y$. The similarity solution is then [3]

$$u \sim u(y/x, z/(yx)^{1/2}). \tag{4}$$

For wavelengths shorter than $\lambda_x \approx y$ the spectrum is bounded by (3) and by the line of horizontal isotropy, $\lambda_z = \lambda_x$, but longer structures are always anisotropic and follow the wake ridge. It was shown in [2, 3] that the structures of the wall-normal velocity *v* are effectively confined to the 'isotropic' region $\lambda_x < y$. Those eddies are detached from the wall, in the sense that the correlation of individual Fourier modes between the logarithmic and the buffer layer is very small. The height over which those correlations are large increases as the structures become longer. The eddies touch the wall when $\lambda_x \approx y$, and the attached eddies beyond that limit are the ones that cluster along the wake ridge.

The nature of the structures generating the wakes is discussed in [4], which studies the vorticity structures in the buffer and logarithmic layers. Vortices are defined as being formed by points in

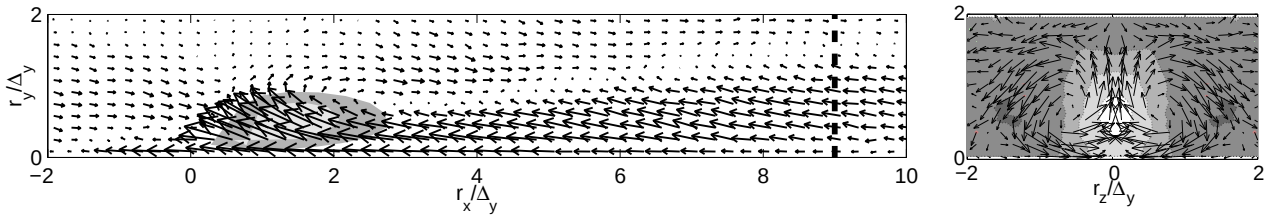

Figure 6: The left plot shows the perturbation velocity field, $(u-U(y),v)$, conditioned on the presence of a vortex cluster, on the $x-y$ plane bisecting the bounding box of the cluster. The shaded area is the probability density function of finding a vortex. The right-hand plot is a section of the conditioned field in the cross plane marked in the left figure. The shaded contours are the perturbation streamwise velocity; $u-U(y)=-0.3(0.1)0.1$. $Re_\tau=550$. Only clusters with $y^+_{max}>100$ are included.

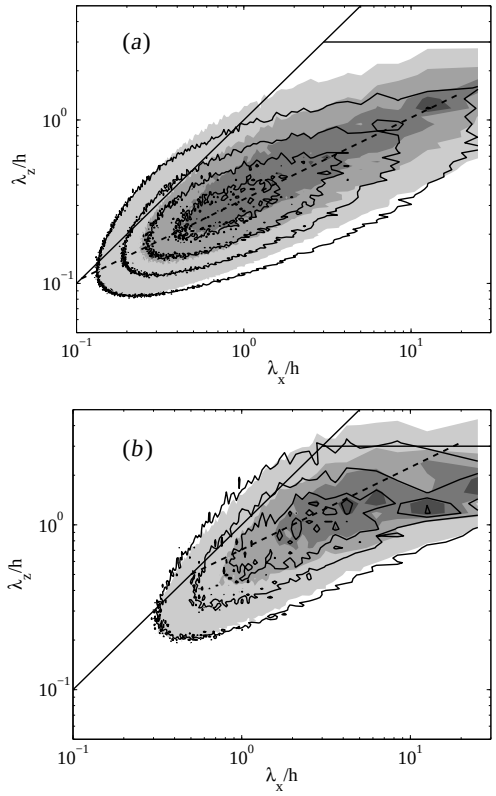

Figure 5: Two-dimensional spectral energy density k_xk_zE/u_τ^2. $Re_\tau=934$. The solid diagonal is $\lambda_z=\lambda_x$. The solid horizontal line is $\lambda_z=3h$, and the dashed diagonal is $\lambda_z=(y\lambda_x)^{1/2}$. The shaded contours are the streamwise velocity; the lines are the Reynolds stress. $(a)\ y/h=0.1$. $(b)\ y/h=0.5$.

which the discriminant D of the velocity gradient tensor is larger than a properly-defined threshold [6]. Connected sets of such points are collected into individual vortex clusters, which break naturally into two distinct groups according to whether their lowest points are above or below a critical level around $y^+\approx 20$. We will call the latter group attached and the former detached. The most interesting clusters are those attached to the wall and reaching into the logarithmic layer, above $y^+=100$. When each of them is inscribed into a parallelepipedal box aligned to the coordinate directions, the boxes are self-similar, with dimensions $\Delta_z\approx 1.5\Delta_y$ and $\Delta_x\approx 3\Delta_y$. Note that for attached clusters it makes sense to associate Δ_y with the height y, because y_{min} is small. When this is done, and when Δ_x and Δ_z are also equated to the streamwise and spanwise wavelengths, the dimensions of the bounding boxes roughly coincide with the location of the spectral peak for the wall-normal velocity v. The vortices themselves appear to be arranged as surfaces or shells within the boxes; while the volume of the bounding box increases as Δ_y^3, the volume contained in points classified as vortices increases only as Δ_y^2.

A conditionally-averaged flow field, based on the centres of the vortex boxes, and scaled with their vertical dimensions, shows a strong v ejection surrounded by two counterrotating vortices, as in a classical hairpin. The antisymmetry is only statistical and, as in the case of the buffer-layer vortices [28], there is little evidence for symmetry in individual vortex clusters.

When the conditionally-averaged flow field is extended down- and up-stream from the location of the vortex box, the result is that in figure 6. In the $x-y$ streamwise plane bisecting the mean location of the box, the presence of a streamwise-velocity structure linked to the vortex cluster is clear. Its location with respect to the cluster is consistent with that of a wake. If we assume that the cluster is advected with the mean velocity at its centre of gravity, the flow closer to the wall is slower than the cluster, and the wake is *behind* the cluster. Above the centre of gravity, the mean flow is faster than the vortices, and the wake is *in front* of the cluster. The averaged vortical structure of the ramp in the transverse plane is shown in the right part of figure 6. It has two counterrotating vortices which are much larger than the size of the original vortex packet, and which are reminiscent of the downstream structure of the wake of a transverse jet in a boundary layer [8].

Similar ramp-vortex structures have been observed by previous investigators [1, 5], with geometric characteristics similar to those found here, but the present interpretation of their relation with the vortex packets is, to our knowledge, new. The results in [4] suggest that the shear layer which defines the top of the ramp is associated with detached vortex clusters, while the attached clusters are only found at the ramp origin. Note for example the absence of any coherent flow structure upstream of the vortex box in figure 6(a), except in the buffer layer. When the conditioned flow field is computed for the detached vortex clusters, the low-speed region extends symmetrically upstream and downstream of the box.

It is interesting to note that the above description is not restricted to 'real' vortices, but that it still holds when the flow is filtered to larger scales (up to $200\times 40\times 100$ wall units in our experiments). Individual vortices are then smoothed, and what remains is only the integrated circulation over fairly large volumes. The velocity perturbations due to the ramps are of the order of u_τ, and the total projected surface of the boxes bounding the wakes is enough to cover the whole wall with some overlap. The perturbation due to the wakes is therefore a substantial fraction of the total perturbation energy in the channel, as could be deduced from the spectra in figure 5.

Those spectra suggest that the wakes widen along the ridge (3) until $\lambda_z \approx 2h$. This effectively determines the longest wavelength in the spectrum, which is

$$\lambda_{x,max}/h \approx 4h/y. \tag{5}$$

This limit is longest at the bottom of the logarithmic layer, where $y^+ \approx 100$ and $\lambda_{x,max}/h \approx Re_\tau/20$. These are very long structures that, even taking into account possible numerical factors, point to hundreds of boundary-layer thicknesses at high Reynolds numbers. Spectral peaks of the order of $20h$ have been documented in experiments [12, 19], and they are probably limited by the length of the experimental records. The present simulations only reach to $\lambda_x \approx 25h$ and, although longer to our knowledge than any other available simulation, they are not long enough to settle the matter. The one-dimensional streamwise premultiplied velocity spectra at the bottom of their logarithmic layers are still essentially flat at their longest wavelengths, as seen in figure 5(a). On the other hand, numerical experiments with shorter simulation boxes show very little difference in the part of the spectrum that is resolved by the simulations [3], suggesting that those very long structures are essentially passive and do not feed into the shorter ones. We have already noted that a short simulation box models long scales as being infinitely long, and the previous results suggest that, given enough time to randomize, structures longer than about $5h$ behave as if they were dynamically infinite.

The shortening of the spectra above the lower logarithmic layer predicted by (5) had been previous noted experimentally, although without explanation [12, 19, 22].

An interesting question is whether the vortex clusters and the ramps discussed here are features of the whole logarithmic layer, or just of its lower edge. The probability density function $p(\Delta_y)$ for the dimensions of the attached vortex clusters collapses well in wall units for different Reynolds numbers, with a maximum around $\Delta_y^+ = 50$. This suggests that the clusters are buffer-layer phenomena which should become negligible for most of the logarithmic layer when Re_τ is large enough, but this is not necessarily so, and depends on the behaviour of $p(\Delta_y)$. The projected area of each vortex cluster on the plane of the wall is $\Delta_x\Delta_z \approx 5\Delta_y^2$, and for any p.d.f. decaying slower than Δ_y^{-2} the largest clusters would be the ones covering most area. This would for example be the case for the distribution $p(\Delta_y) \sim \Delta_y^{-1}$, which was suggested in [27] on similarity grounds. In our simulations the decay of $p(\Delta_y)$ depends on the threshold used to define the vortices, and there is little support for a self-similar distribution. But we are conscious of the limited extent of our logarithmic layers, and the matter remains under investigation.

Global modes

The increase with the Reynolds number of the intensity of the streamwise velocity was justified above by noting that the premultiplied energy spectra are approximately flat in the long-wavelength regime, and that they become longer as Re_τ increases. Since the total energy is the integral with respect to $\log(\lambda_x)$ of the premultiplied spectrum, and since λ_x ranges between limits which scale respectively in wall and in outer units, it follows that u'^{+2} should increase as $\log(h^+) = \log(Re_\tau)$. This is the dashed line drawn in figure 2.

The same argument does not hold when comparing flows at a given value of y/h. The shorter end of the energy spectrum in the logarithmic and outer layers is the intersection of the wake line (3) with the isotropic locus $\lambda_x = \lambda_z$, which happens at $\lambda_x \approx y$. This is confirmed by the numerical spectra, as well as by the experimental limits of the classical k^{-1} spectrum [27]. The long-wavelength end is given by (5), and the range of the

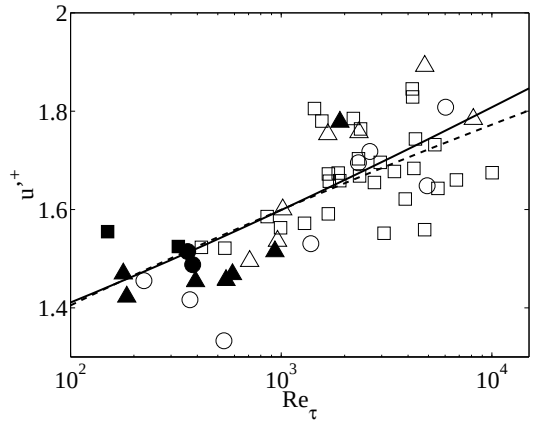

Figure 7: Scaling of the total energy of the streamwise fluctuations, as a function of the Reynolds number. $y/h = 0.4$. □ , boundary layers; ○ , channels; △ , pipes. Open symbols are laboratory experiments, and closed ones are computations. ——— , $u'^{+2} \sim 1 + \alpha U_c^{+2}$; – – – – , $u'^{+} \sim \log Re_\tau$ [7].

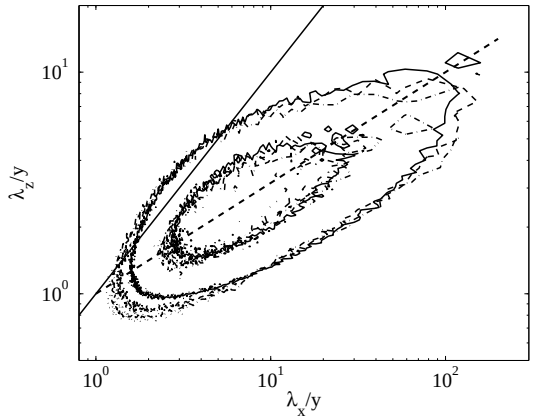

Figure 8: Premultiplied cospectra of the Reynold stress in the logarithmic layer, as a function of λ/y. ——— , $y/h = 0.1$; – – – – , $y/h = 0.15$; —·— , $y/h = 0.2$. $Re_\tau = 934$.

spectral integral is therefore

$$\lambda_{x,max}/\lambda_{x,min} \approx 4h^2/y^2, \tag{6}$$

which is independent of Re_τ. If the magnitude of the spectrum scales with u_τ^2, arguments like this one allow us to estimate how u'^2 depends on y/h, but they support the scaling of u' with u_τ.

On the other hand, the experimental and numerical evidence compiled in figure 7 suggests that also in the the outer layer the scaling of the fluctuations with u_τ fails to apply [7].

The classical argument for the scaling of u' is that, since the total Reynolds stress is given by the momentum equation (in a channel) as $u_\tau^2(1-y/h)$, and since the stress has to be carried by the product $\langle u'v'\rangle$, the easiest assumption is that both u' and v' scale with u_τ. It was however noted by Townsend [31] that this argument does not apply to 'inactive' eddies which carry no Reynolds stresses. We already found such eddies in the upper edge of the buffer-layer spectra in figure 4, and it is clear from the observation of the higher contours of the energy spectra and of the Reynolds stress cospectra in figure 5, that the longest and widest eddies in the outer flow are also inactive.

There is a second argument that also supports the scaling $u' \sim u_\tau$. Assume an eddy of the self-similar family, $y_{max} \sim y_{min} \sim y$.

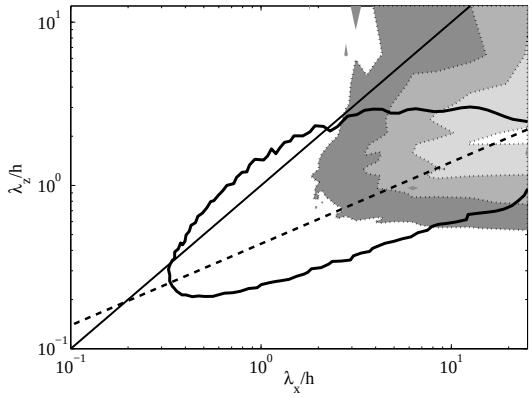

Figure 9: Correlation height for individual Fourier modes of the streamwise velocity. Contours are $H_{uu}/h = 0.6(0.1)0.9$. The $k_x k_z E_{uu}$ spectrum at $y = h/2$ is included for comparison. $Re_\tau = 550$.

If we think of the perturbation in u as coming from the mixing of the mean velocity profile, such as in the right-hand side of figure 6, we can estimate the perturbation generated by such an eddy as $u' \approx U(y_{max}) - U(y_{min})$, which in the logarithmic layer is approximately $u_\tau \log(y_{max}/y_{min})$. This also scales in wall units and, in conjunction with the argument in the previous paragraph, suggests that the Reynolds stress is carried in the logarithmic layer by self-similar eddies. This is supported by the cospectra in figure 8, which collapse well in terms of λ/y near their active peak, while the collapse deteriorates for the relatively-inactive shorter and longer wavelengths.

When the mixing argument is applied to attached modes, which are correlated from the wall to a given height y, it suggests that those modes should scale with $U(y)$ instead of with u_τ, especially if they are inactive. This argument would apply to all the wider modes in the logarithmic layer, but for most of them the experimental or numerical data is too scant to check the prediction.

There is however a set of modes in which the test can be carried, and for which there are results at high Reynolds numbers from laboratory experiments. Consider the correlation coefficient for a particular Fourier mode $\widehat{u}$ at two heights,

$$C_{uu}(k_x, k_z, y, y') = \frac{|\langle \widehat{u}(k_x, k_z y) \widehat{u}^*(k_x, k_z, y') \rangle|}{(\langle |\widehat{u}(k_x, k_z, y)|^2 \rangle \langle |\widehat{u}(k_x, k_z, y')|^2 \rangle)^{1/2}}. \quad (7)$$

This is a real number between zero and one, which would be equal to unity for all y and y' if that particular mode where fully correlated across the full channel. We can define a 'correlation height',

$$H_{uu}^2(k_x, k_z) = \int_0^h \int_0^h C_{uu} \, \mathrm{d}y \, \mathrm{d}y', \quad (8)$$

which characterizes the depth over which the particular Fourier mode is correlated. In general H_{uu} increases as the wavelengths become longer and wider (see figure 9) and, for $\lambda_x \gtrsim 6h$ all the modes are essentially correlated over the full half-channel. These global modes are particularly easy to analyse, because they do not interfere with any shallower structures at the same scales. A reference to figure 5 shows that they carry little Reynolds stress, and the previous argument suggests that they should scale with the centreline velocity U_c, instead of with u_τ. Also, because the high correlation region in figure 9 spans most spanwise wavelengths, their intensity can be computed from laboratory spectra, which usually do not have spanwise information.

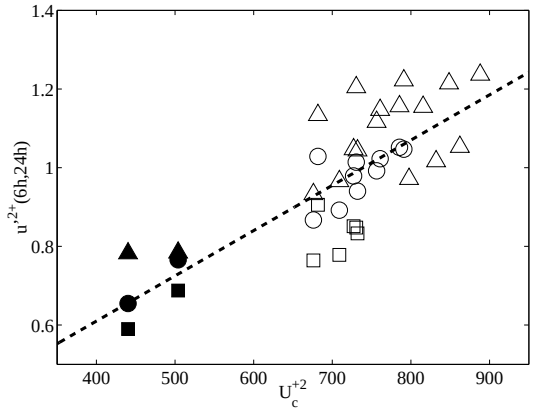

Figure 10: Scaling of the energy in the 'global' modes, $6 < \lambda_x/h < 24$, for numerical channels (solid symbols) and experimental boundary layers and pipes (open symbols). $\triangle$, $y/h = 0.1$; $\circ$, $y/h = 0.2$; $\square$, $y/h = 0.3$. The dashed line goes through the origin.

This scaling is tested in figure 10, which plots the energy in the band $6 < \lambda_x/h < 24$ as a function of the Reynolds number, and at three wall distances. Besides the numerical channels, the plot contains data from experimental boundary layers [10] and pipes [26]. The failure of the classical scaling is clear from the figure, and the proposed scaling with U_c^2 works well.

We can now get back to the scaling failure of the total velocity fluctuations in figure 7. Since there is an active part of the spectrum which scales as u_τ^2, and an inactive one which scales like U_c^2, we can expect that the total scales as $u'^{+2} \sim 1 + \alpha U_c^{+2}$, which is the solid straight line in the figure. A different scaling $u' \sim \log(Re_\tau)$ was proposed in [7] to fit the data, and it is also included in the figure. Even within the fairly wide range of Reynolds numbers compiled in figure 7, both scalings differ little, and it is unlikely that they will ever be distinguished through global measurements alone. They however predict different asymptotic behaviours at very large Reynolds numbers, and observations like the present one on the scaling of partial spectral ranges offer the best hope of deciding which argument is correct.

Conclusions

We have briefly reviewed the present status of the understanding of the dynamics of turbulent flows near smooth walls, and given rational explanations for several of the scaling failures detected in experiments. This is a subject that, like most others in turbulence, is not completely closed, but which has evolved in the last two decades from empirical observations to relatively coherent theoretical models. It is also one of the first cases in turbulence, perhaps together with the structure of small-scale vorticity in isotropic turbulence, in which the key technique responsible for cracking the problem has been the numerical simulation of the flow.

The reason for the successes in the buffer layer is undoubtedly that the Reynolds numbers of the important structures are low, and therefore easily accessible to computation, while experiments are difficult.

The study of the logarithmic layer, on the other hand, requires massive computations at realistic Reynolds numbers, which only now are becoming available. It is in this area where the cost of computations and of laboratory experiments have to be weighted against their respective advantages. It is probably true

that both will forever be complementary. Note that we have used data from both sources whenever possible. But it is no longer true that Reynolds number alone is what separates ones from the others.

Acknowledgements

The preparation of this paper was supported in part by the CICYT grant DPI2003–03434. The computer time needed for the $Re_\tau = 550$ and 1880 simulations was made available by the CEPBA/IBM centre of the Universidad Politécnica de Catalunya. We are most grateful to P. Zandonade and R.D. Moser for providing us with the raw data from the $Re_\tau = 934$ simulation.

References

[1] Adrian, R.J., Meinhart, C.D. and Tomkins, C.D. Vortex organization in the outer region of the turbulent boundary layer, *J. Fluid Mech.* **422**, 1–54 (2000)

[2] del Álamo, J.C. and Jiménez, J., Spectra of very large anisotropic scales in turbulent channels, *Phys. Fluids* **15** L41–L44 (2003)

[3] del Álamo, J.C., Jiménez, J., Zandonade, P. and Moser, R.D., Scaling of the energy spectra of turbulent channels, *J. Fluid Mech.* **500**, 135–144 (2004)

[4] del Álamo, J.C., Jiménez, J., Zandonade, P. and Moser, R.D., Self-similar vortex clusters in the attached logarithmic region, submitted *J. Fluid Mech.*

[5] Christensen, K.T. and Adrian, R.J., Statistical evidence of hairpin vortex packets in wall turbulence, *J. Fluid Mech.* **431**, 433–443 (2001)

[6] Chong, M.S., Perry, A.E. and Cantwell, B.J., A general classification of three-dimensional flow fields, *Phys. Fluids* A **2**, 765–777 (1990)

[7] DeGraaf, D.B. and Eaton, J.K., Reynolds number scaling of the flat-plate turbulent boundary layer, *J. Fluid Mech.* **422**, 319–346. (2000)

[8] Fric, T.F. and Roshko, A., Vortical structure in the wake of a transverse jet, *J. Fluid Mech.* **279**, 1–47 (1994)

[9] Hamilton, J. M., Kim, J. and Waleffe, F., Regeneration mechanisms of near-wall turbulence structures. *J. Fluid Mech.* **287**, 317–348 (1995)

[10] Hites, M.H., Scaling of high-Reynolds turbulent boundary layers in the national diagnostic facility. Ph.D. thesis, Illinois Institute of Technology (1977)

[11] Jeong, J., Hussain,F., Schoppa,W. and Kim,J., Coherent structures near the wall in a turbulent channel flow. *J. Fluid Mech.* **332**, 185–214 (1997)

[12] Jiménez, J., The largest structures in turbulent wall flows. In *CTR Annual Research Briefs*, 943–945. Stanford University (1998)

[13] Jiménez, J., Computing high-Reynolds-number turbulence: will simulations ever replace experiments?, *J. of Turbulence* **22** (2003)

[14] Jiménez, J., del Álamo, J.C. and Flores, O., The large-scale dynamics of near-wall turbulence, *J. Fluid Mech.* **505**, 179–199 (2004)

[15] Jiménez, J., Kawahara, G., Simens, M.P., Nagata, M. and Shiba, M., Characterization of near-wall turbulence in terms of equilibrium and 'bursting' solutions, submitted to *Phys. Fluids*.

[16] Jiménez, J. and Moin, P., The minimal flow unit in near wall turbulence. *J. Fluid Mech.* **225**, 221–240 (1991)

[17] Jiménez, J. and Pinelli, A., The autonomous cycle of near wall turbulence, *J. Fluid Mech.* **389**, 335–359 (1999).

[18] Jiménez, J. and Simens, M.P., Low-dimensional dynamics in a turbulent wall flow, *J. Fluid Mech.* **435**, 81–91 (2001).

[19] Kim, K. C. and Adrian, R. J., Very large-scale motion in the outer layer. *Phys. Fluids A* **11**, 417–422 (1999)

[20] Kim, J. and Hussain, F., Propagation velocity of perturbations in channel flow. *Phys. Fluids* A **5**, 695–706 (1993)

[21] Kim, J., Moin, P. and Moser, R., Turbulence statistics in fully developed channel flow at low Reynolds number. *J. Fluid Mech.* **177**, 133–166 (1987)

[22] Lawn, C.J., The determination of the rate of dissipation in turbulent pipe flow, *J. Fluid Mech* **48**, 477-505 (1971)

[23] Moin, P. and Mahesh, K., Direct numerical simulation: A tool in turbulence research, *Ann. Rev. Fluid Mech.* **30** 539–578 (1998)

[24] Moser, R.D., Kim, J. and Mansour, N.N., Direct numerical simulation of turbulent channel flow up to $Re_\tau = 590$, *Phys. Fluids* **11**, 943–945 (1999)

[25] Österlund, J.M., Johansson, A.V., Nagib, H.M. and Hites, A note on the overlap region in turbulent boundary layers, *Phys. Fluids* **12**, 1–4 (2000)

[26] Perry, A.E. and Abell, C.J., Scaling laws for pipe-flow turbulence. *J. Fluid Mech.* **67**, 257–271 (1975)

[27] Perry, A.E., Henbest, S. and Chong, M.S., A theoretical and experimental study of wall turbulence. *J. Fluid Mech* **165**, 163–199 (1986)

[28] Robinson, S.K., Coherent motions in the turbulent boundary layer. *Ann. Rev. Fluid Mech.* **23**, 601–639 (1991)

[29] Smith, C.R. and Metzler, S.P., The characteristics of low speed streaks in the near wall region of a turbulent boundary layer. *J. Fluid Mech.* **129**, 27–54 (1983)

[30] Tennekes, H. and Lumley, J.L., *A first course in turbulence*, chapter 8. MIT Press (1972)

[31] Townsend, A. A. *The structure of turbulent shear flows*, 2nd edn. Cambridge U. Press (1976)